EARTH SURFACE PROCESSES AND LANDFORMS
Earth Surf. Process. Landforms **40**, 1574–1586 (2015)

Published online 17 April 2015 in Wiley Online Library
(wileyonlinelibrary.com) DOI: 10.1002/esp.3735

Fluid flow and sediment entrainment in the Garonne River bore and tidal bore collision

Claire E. Keevil,[1] Hubert Chanson[2]* and David Reungoat[3]
[1] Department of Geography, Environment and Earth Sciences, University of Hull, Hull HU6 7RX, UK
[2] School of Civil Engineering, The University of Queensland, Brisbane, QLD 4072, Australia
[3] I2M, Laboratoire TREFLE, Université de Bordeaux, 16 avenue Pey-Berland, CNRS UMR 5295, 33607 Pessac, France

Received 31 December 2014; Revised 25 February 2015; Accepted 26 February 2015

*Correspondence to: Hubert Chanson, The University of Queensland, School of Civil Engineering, Brisbane QLD 4072, Australia. E-mail: h.chanson@uq.edu.au

ESPL
Earth Surface Processes and Landforms

ABSTRACT: A detailed field study was carried out on a tidal bore to document the turbulent processes and sediment entrainment which occurred. The measured bore, within the Arcins Channel of the Garonne River (France), was undular in nature and was followed by well-defined secondary wave motion. Due to the local river geometry a collision between the Arcins channel tidal bore and the bore which formed within the main Garonne River channel was observed about 800 m upstream of the sampling site. This bore collision generated a transient standing wave with a black water mixing zone. Following this collision the bore from the main Garonne River channel propagated 'backward' to the downstream end of the Arcins channel. Velocity measurements with a fine temporal resolution were complemented by measurements of the sediment concentration and river level. The instantaneous velocity data indicated large and rapid fluctuations of all velocity components during the tidal bore. Large Reynolds shear stresses were observed during and after the tidal bore passage, including during the 'backward' bore propagation. Large suspended sediment concentration estimates were recorded and the suspended sediment flux data showed some substantial sediment motion, consistent with the murky appearance of the flood tide waters. Copyright © 2015 John Wiley & Sons, Ltd.

KEYWORDS: tidal bore; Garonne River; sediment processes; field observations; bore collision

Introduction

A tidal bore is a hydraulic jump in translation propagating upstream in an estuarine zone, when the tidal flow turns to rising (Tricker, 1965; Peregrine, 1966; Liggett, 1994). It is a rapidly-varied unsteady open channel flow generated by the relatively rapid rise in water elevation during the early flood tide, when the tidal range exceeds 4.5 m to 6 m and the funnel shape of both river mouth and lower estuarine zone amplifies the tidal wave (Lighthill, 1978; Chanson, 2011a). Figure 1 illustrates tidal bores in China and France, and pertinent accounts include Moore (1888) and Malandain (1988). Figure 1(A) shows the undular bore of the Dordogne River (France), which joins the Garonne River downstream off the City of Bordeaux. Figure 1(B) presents a rare sight of tidal bore crossing in the Qiantang River (China), illustrating the impact of bore crossing on sediment processes.

There has been relatively little investigation to date of the impact of tidal bores on sedimentary processes. Laboratory studies of tidal bores carried out to date have been conducted without suspended sediments, however recent results highlight their importance to erosional processes (Macdonald *et al.* 2009; Chanson 2011b; Khezri and Chanson, 2012a). One study on sediment scour used clear-water with a live bed to study the scour inception process (Khezri and Chanson, 2012b). Data from field studies have demonstrated the massive impact of tidal bores on sedimentary processes, e.g. suspended sediment transport, bed load, scour and erosion (Bartsch-Winkler *et al.* 1985; Faas, 1995; Chanson *et al.*, 2011). However, it is challenging to compare data from these different studies due to the differences in hydrodynamic conditions and sediment characteristics (Table I). Altogether recent findings suggest that (a) the passage of tidal bore is associated with intense sediment scouring and suspension of bed materials (Greb and Archer, 2007; Khezri and Chanson, 2015), (b) the tidal bore advance may contribute to channel shifting in flat and wide bays (Chanson, 2011a), and (c) the very early flood flow may be characterised by very high suspended sediment concentrations (Chanson *et al.* 2011; Furgerot *et al.*, 2013; Fan *et al.*, 2014). Field data exhibited on the other hand different results and trends depending upon the nature of sediment materials (cohesive, non-cohesive, mixture), the site location (e.g. river mouth, inland), site topography (shallow-water bay, constrained river bed), tidal conditions (spring, neap tides) and fluvial discharge (drought, flood).

The collision and crossing of tidal bores have been observed in a small number of river systems, where the flow of the incoming flood tide has been split. In Hangzhou Bay (China), the Qiantang River bore develops in two distinct channels: the northern and southern channels. When these channels merge, the previously separate bores cross at a near right angle with spectacular splashing and mixing (Figure 1(B)). At the intersection of the two bores, a very turbulent wake region is seen in which the water surface is nearly black, suggesting

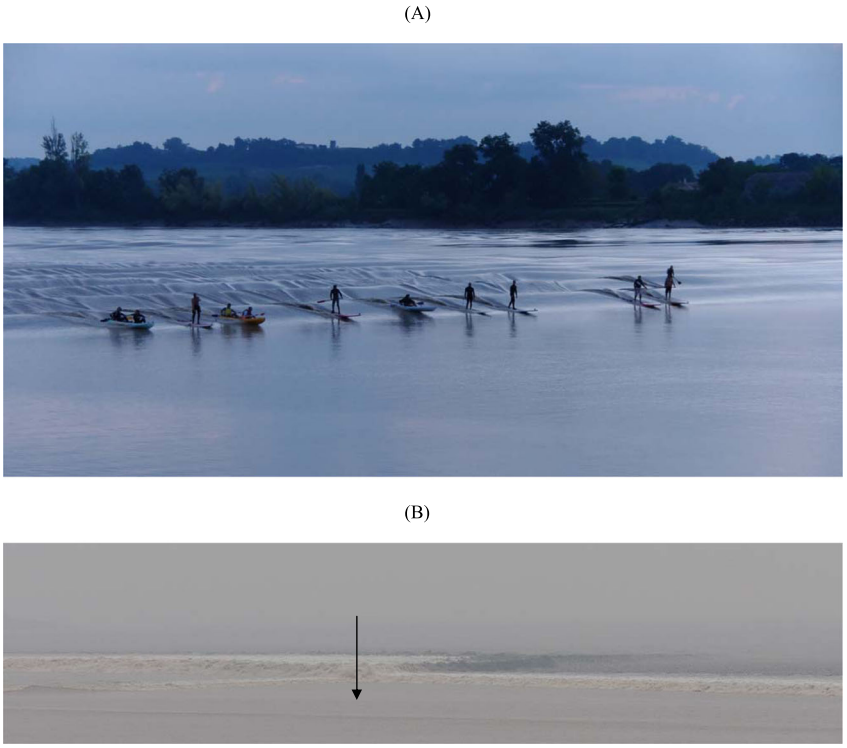

Figure 1. Photographs of tidal bores. (A) Undular tidal bore of the Dordogne River on 24 August 2012 at St Pardon (France). (B) Qiantang River bore crossing on 6 September 2013 upstream of Daquekou (China), viewed from the left bank: the arrow points to the bore intersection. This figure is available in colour online at wileyonlinelibrary.com/journal/espl

some intense sediment upwelling in the water column. In shallow water bays, a tidal bore may propagate at different speeds in the braided channels, leading occasionally to some tidal bore collision (e.g. Bay of Mont Saint Michel, France; Kent River estuary, UK). Rowbotham (1983) described the bore of the River Severn advancing at different speeds when split into two channels at Gloucester: 'at the upper end of Alney Island'; 'the western bore [...] split with much confusion'; 'part runs down the East Channel and may go as far as the one time Globe Inn at Sandhurst before meeting its tardy brother face to face. After a swirling struggle for supremacy the upward tide inevitably wins' (Rowbotham 1983, 21–22). There are anecdotal mentions of frontal collision of tidal bores, in the River Trent (UK) and Garonne River (France) (Reungoat et al., 2014a). On 6 November 2013, several surfers riding the Petitcodiac River tidal bore (Moncton, Canada) experienced a bore collision, allegedly linked with an upstream reservoir release travelling downstream and colliding head-on with the natural tidal bore (CBC News, 2013). The surfers were pushed back nearly 300 m by the colliding bore: 'During a 10-minute period, the three surfers were caught in a series of whirling currents provoked by the collision of the super bore and the opposing currents [...]; After some time they managed to break free and make it to shore safe and sound'. The collision of undular bores was analysed theoretically by Bestehorn and Tyvand (2009). The phenomenon is identical to an undular bore impacting a solid vertical wall when both bores have the same strength (Stoker, 1957; Ramsden, 1996), but the development of Bestehorn and Tyvand (2009) was expanded to bores of different strengths.

Field measurements of tidal bores are currently very limited, although there have been a few studies published to date (Table I). Table I summarises a number of key field studies, highlighting the diversity in instrumentation and flow conditions. Herein new field measurements were conducted on the Garonne River bore (France). Velocity and sediment properties were recorded prior to, during and after passage of the tidal bore in the secondary channel of the Garonne River, and the data were complemented with continuous measurements of water conductivity, temperature and sediment concentration. An unusual feature of the study was the influence of the bore of the main channel of the Garonne River which entered the upstream end of the channel and collided with the main tidal bore. The findings yield a better understanding of the sediment processes in tidal bore-affected rivers, including the effects of tidal bore collision.

Methods

Study site and instrumentation

The field study was conducted in the Arcins channel of the Garonne River (France), about 6.5 km south-west of the centre of the City of Bordeaux. The same site was previously used by Chanson *et al.* (2011) and Reungoat *et al.* (2014a) (Table I). The channel is 1.8 km long, 70 m wide and about 1.1 to 2.5 m deep at low tide (Figures 2 and 3). Figure 2(A) shows a photograph of the channel. Figure 2(B) presents a cross-sectional survey conducted on 19 October 2013, in which data are compared with the bathymetric surveys conducted at the same location on 10 September 2010 and 7 June 2012. The survey data indicated some channel siltation since the latest field study. The field measurements were conducted under spring tide conditions on 19 October 2013 afternoon when the tidal range in Bordeaux was 6.09 m. All measurements were made from the hull of a heavy and sturdy pontoon (Figure 2(C)) (0° 31′ 06.5" W, 44° 47′ 58.6" N). Figure 3 presents a plan view map of the site.

A D&A Instrument™ OBS-5+ (Serial No S5153, Firmware v1.20) unit recorded the suspended sediment concentration about 0.55 m below the water surface. The optical backscatter

Table I. Field measurements of tidal bores

Reference	Initial flow V_1 m/s	d_1 m	Instrument	Channel geometry	Remarks
Lewis (1972)	0 to +0.2	03.9 to 1.4	Hydro-Products™ type 451 current meter	Dee River (UK) near Saltney Ferry footbridge. Trapezoidal channel	Field experiments between March and September 1972.
Navarre (1995)	0.65 to 0.7	1.12 to 1.15	Meerestechnik-Electronik GmbH model SM11J acoustic current meter (sampling 10Hz)	Dordogne River (France) at Port de Saint Pardon Width ~ 290 m	Field experiments on 25 and 26 April 1990.
Kjerfve and Ferreira (1993)			Interocean™ S4 electro-magnetic current meters (sampling: 1-2 Hz)	Rio Mearim (UK)	Field experiments on 19–22 Aug. 1990 and 28 Jan.–2 Feb. 1991.
Wolanski *et al.* (2001)	–	0.45	Analite™ nephelometer	Ord River (East Arm) (Australia) Width ~ 380 m	Field experiments in August 1999.
Chen (2003)	–	–	–	North Branch of the Changjiang River Estuary (China)	Experiments in April 2001.
Simpson *et al.* (2004)	0.1	~0.8	ADCP (1.2 0 MHz) (sampling rate:1 Hz)	Dee River (UK) near Saltney Ferry Bridge. Trapezoidal channel (base width ~ 60 m)	Field experiments in May and September 2002.
Wolanski *et al.* (2004)	0.15	1.5 to 4	Nortek™ Aquadopp ADCP (sampling rate:2 Hz)	Daly River (Australia). Width ~ 140 m	Field experiments in July and September 2002, and on 2 July 2003.
Fan *et al.* (2014)	–	–	Sediment cores	Qiatang River (China)	Field works in May 2010.
Chanson *et al.* (2011)			ADV Nortek™ Vector (6 MHz) (sampling: 64 Hz)	Arcins channel, Garonne River (France) Width ~ 76 m	Undular tidal bore.
	0.33	1.40 (*)			10 Sept. 2010.
	0.30	1.43 (*)			11 Sept. 2010.
Mouaze *et al.* (2010)			ADV Nortek™ Vector (6 MHz) (sampling: 64 Hz)	Pointe du Grouin du Sud, Sélune River (France)	Breaking tidal bore.
	0.86	0.15 (*)			24 Sept. 2010.
	0.59	0.11 (*)			25 Sept. 2010.
Furgerot *et al.* (2013)	0.4	0.75	ADV Nortek™ Vector (6 MHz) (sampling: 64 Hz)	Sée River (France) Width ~ 22 m	Undular bore on 7 May 2012.
Reungoat *et al.* (2014a)			microADV Sontek™ (16 MHz) (sampling: 50 Hz)	Arcins channel, Garonne River (France) Width ~ 78 m	Weak undular tidal bore.
	0.68	2.0 (*)			7 June 2012 morning
	0.59	1.94 (*)			7 June 2012 afternoon
Present study	0.26	1.32 (*)	ADV Nortek™ Vectrino + (10 MHz) (sampling: 200 Hz)	Arcins channel, Garonne River (France) Width ~ 65 m	Undular tidal bore on 19 October 2013 afternoon.

d_1: initial water depth (at sampling location); V_1: initial flow velocity; (–): information not available; (*): equivalent depth A_1/B_1.

(A)

(B)

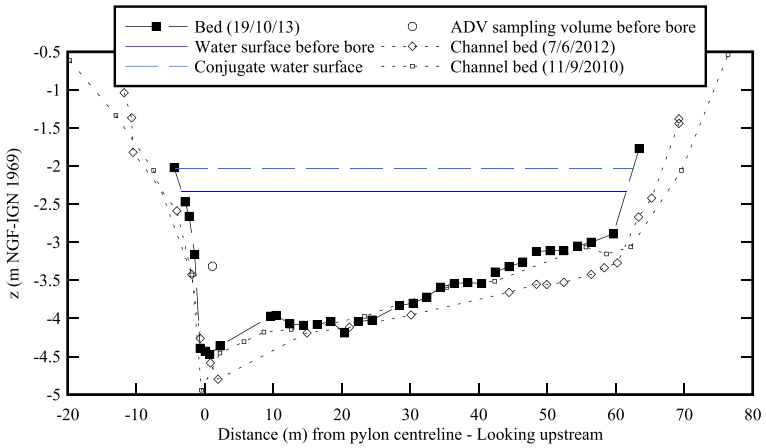

(C)

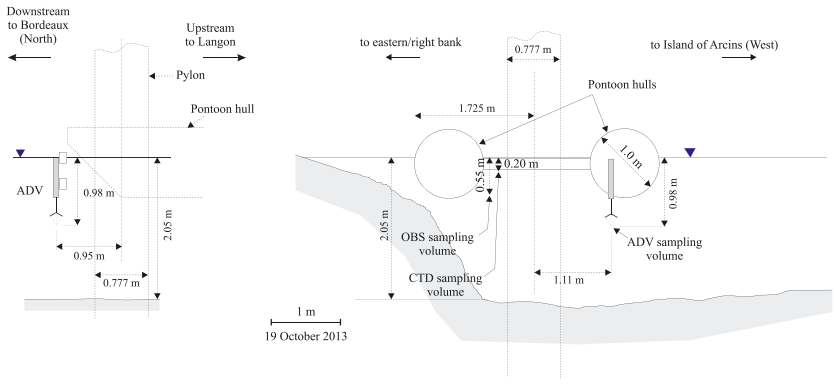

Figure 2. Sampling location in the Arcins channel, with surveyed cross-section at low tide water level on 19 October 2013. (A) Tidal bore passing the sampling site. Surfers towards Arcins Island were on the bore front. Sampling carried out from the pontoon fixed on the eastern bank (foreground) of the Arcins Channel (B) Distorted cross-sectional survey looking upstream (i.e. south) with the eastern/right bank on the left. Comparison with the 2010 and 2012 surveys at the same cross-section and water levels immediately before and after the bore. (C) Un-distorted dimensioned sketch of the ADV mounting, sampling volume location and water surface 5 minutes prior to the tidal bore on 19 October 2013- Left: view from Arcins Island – Right: looking upstream (i.e. south). This figure is available in colour online at wileyonlinelibrary.com/journal/espl

(OBS) system was sampled at 25 Hz, with the data returned every 10 s at 25 Hz for 5 s. The water temperature, conductivity and pH were recorded about 0.2 m below the water surface. The water temperature was measured manually with a thermometer (Ebro Electronic™ TT100 Type T) as well as with a conductivity, temperature and depth (CTD) self-logging system Model SBE37-SMP (Serial No 3980, Firmware v2.6) sampling at 0.2 Hz. The water conductivity was recorded also with the CTD unit at 0.2 Hz, as well as with a conductivity meter Consort™ C931. The pH was sampled manually with a waterproof pH meter. The instantaneous velocity components were measured with a Nortek™ ADV Vectrino + (10 MHz, serial number VNO1356), mounted next to the OBS. The acoustic Doppler velocimeter (ADV) system was equipped with a down-looking head (ADV field). The velocity range was 2.5 m/s, the ADV was set up with a transmit length of 0.3 mm and a sampling

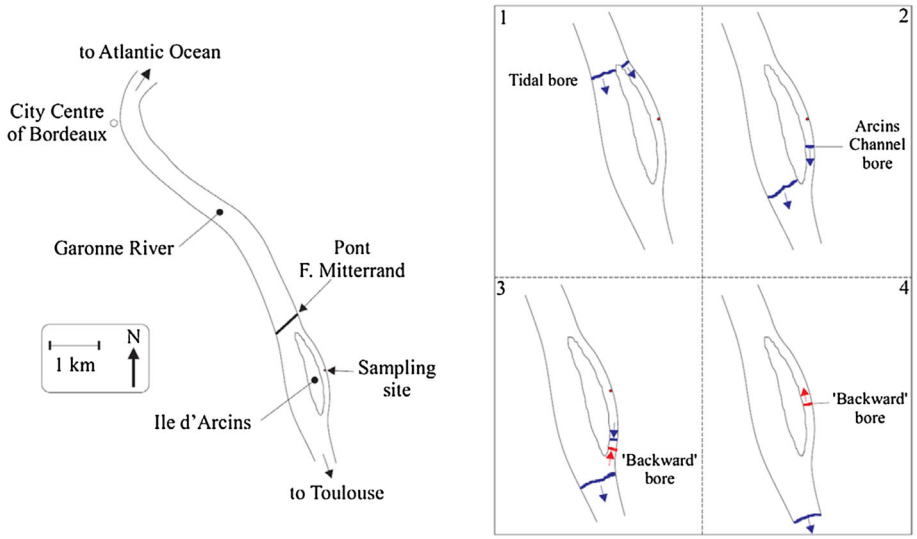

Figure 3. Plan view of the tidal bore propagation around the Arcins Island including formation of the 'backward' bore on 19 October 2013. Right: top view cartoon of bore propagation around the island. This figure is available in colour online at wileyonlinelibrary.com/journal/espl

volume of 1.5 mm height, and the sampling rate was 200 Hz. The ADV data underwent a post-processing procedure to eliminate any erroneous or corrupted data from the data sets (Reungoat *et al.*, 2014b). The percentage of good samples was >82% for the entire data set.

The channel cross-section was surveyed with a Theodolite n"64585 DGT10 CST/berger™. Further observations were recorded with digital single lens reflex (dSLR) cameras and high-definition (HD) digital video cameras.

Characterisation of Sediment Materials

Some Garonne River bed material was collected at low tide on 17, 19 and 20 October 2013 afternoons next to the low tide water line on the eastern bank. The soil samples consisted of fine mud and silt materials. Their granulometry was measured with a Malvern™ laser Mastersizer 2000 equipped with a Hydro™ 3000SM dispersion unit for wet samples. The bed sediment samples were mixed mechanically, the granulometry was performed 15 times with six different data analyses and the results were averaged. The differences between all the runs were negligible.

The rheological properties of mud samples were tested with a Malvern™ Kinexus Pro (Serial MAL1031375) rheometer equipped with a plane-cone (Ø =40 mm, cone angle: 4°). The gap truncation (150 µm) was selected to be more than ten times the mean particle size. The tests were performed under controlled strain rate at a constant temperature (25 °C). Between the sample collection and the tests, the mud was left to consolidate for 4 days. Prior to each rheological test, a small mud sample was placed carefully between the plate and cone. The specimen was then subjected to a controlled strain rate loading and unloading between 0.01 s^{-1} and 1000 s^{-1} with a continuous ramp (two min ramp time).

The calibration of the ADV and OBS units was accomplished by measuring the ADV and OBS signal amplitudes of known, artificially produced concentrations of material obtained from the bed, diluted in tap water and thoroughly mixed. Tap water was selected for simplicity since previous studies showed that the solution (distilled water, tap water, estuarine water) had little effect on the calibration curve of an ADV (Chanson *et al.*, 2008; Reungoat *et al.*, 2014a). Herein two series of experiments were conducted. During the first series, the laboratory experiments were performed with the Nortek™ ADV Vectrino + system and OBS-5+ unit using the same settings as for the field measurements on 19 October 2013. For each test, a known mass of wet sediment (density: 1.341) was introduced in a water tank which was continuously stirred with a paint mixer. The mass of wet sediment was measured with a Mettler™ Type PM200 (Serial 86.1.06.627.9.2) balance. The mass concentration was deduced from the measured mass of wet sediment and the measured water tank volume. The average ADV backscatter amplitude measurements represented the average signal strength of the four receivers, and it was measured in counts. The second series of experiments were conducted with the OBS-5+ unit only and each run lasted five minutes. The mass of wet sediment was recorded with an Adams™ PGW753i scale with a precision of 0.001 g. During all the tests, the suspended sediment concentrations (SSCs) ranged from less than 0.01 kg/m^3 to more than 60 kg/m^3.

In addition, a number of water samples were also collected on 19 October 2013 at 16:45 (prior to the arrival of the bore) and 17:45 (during the flood tide) about 0.2 m below the water surface. The water samples were dried in an oven, set at 41 C, to measure the mass of dry sediments for each sample.

Sediment Characteristics

The relative density of wet sediment samples was $\mathbf{s} = 1.341–1.41$ (Table II), corresponding to a sample porosity of 0.78–0.75 with a density of dry sediments of 2.65, as checked by drying a number of samples. The particle size distribution data presented close results, irrespective of the collection dates and locations. The median particle size was 15 µm corresponding to some silty material (Graf, 1971; Julien, 1995) and the sorting coefficient $\sqrt{d_{90}/d_{10}}$ was about 3.7 (Table II). The bed material was a cohesive mud mixture. The results are compared with previous data at the same site in Table II. The properties of the Garonne River sediments were similar irrespective of the collection date over the 4 year period.

Rheometry tests provided some information on the relationship between shear stress and shear rate of the bed material, during the loading and unloading phases of small mud quantities. The data showed some difference between the loading and unloading phases, typical of some form of material thixotropy, the magnitude of shear stress during the unloading phase being consistently smaller than during the loading for a given shear rate

Table II. Measured properties of sediment samples collected in the Garonne River at Arcins. Comparison with mud samples collected in the Garonne River at Arcins (France) in September 2010 and June 2012 and flood sediment sample during the January 2011 flood of the Brisbane River (Australia)

Ref.	River system	d_{50}	d_{90}	d_{10}	Rheometer	Configuration	Loading	Shear rate Min.	Shear rate Max.	Temperature	Sediment collection data	**s**	τ_c	μ	m
		μm	μm	μm				1/s	1/s	Celsius			Pa	Pa.s	
Present study	Garonne River at Arcins	15.06	4.13	56.93	Malvern™ Kinexus Pro	Cone 40 mm 4° (smooth)	Continuous ramp	0.01	1000	25.0	19 October 2013	1.341	6.38	3.13	0.286
													6.21	4.76	0.278
													6.17	5.00	0.271
													6.61	5.31	0.268
													5.48	4.28	0.278
													4.77	4.39	0.276
Reungoat *et al.* (2014a)	Garonne River at Arcins	12.7	3.35	50.0	Malvern™ Kinexus Pro	Cone 40 mm 4° (smooth)	Continuous ramp	0.01	1000	25.0	7 June 2012	1.357	75.4	36.1	0.22
											8 June 2012	1.428	15.7	11.4	0.27
											8 June 2012		21.5	13.1	0.28
						Disk 20 mm (smooth)	Continuous ramp	0.01	1000	25.0	7 June 2012	1.357	271	17.5	0.40
											8 June 2012	1.428	74.2	2.87	0.60
Chanson *et al.* (2011)	Garonne River at Arcins	–	–	–	TA-ARG2	Cone 40 mm 2° (smooth)	Steady state flow steps	0.01	1000	20	11 Sept. 2010	1.41	49.7	44.6	0.28
													61.4	52.9	0.27
Brown and Chanson (2012)	Brisbane River in flood at Gardens Point Road	26.3	2.96	85.95	Mettler™ Viscosimeter	Cylindrical (0.59 mm between cylinders)		0	1045	25	14 Jan. 2011	1.46	35.5	8.1	0.34

d_{50}: median grain size; **s**: specific density; τ_c: apparent yield stress; μ: apparent effective viscosity; m: Herschel–Bulkley law exponent (Equation (1)).

(Reungoat *et al.*, 2014b). The rheometer data were used to estimate an apparent yield stress τ_c and effective viscosity μ of the sediment material. Although a complete characterization of a thixotropic material would require the determination of all parameters of a thixotropic model, a rapid, more approximate characterisation of the material was used. The apparent yield stress and effective viscosity were estimated by fitting the rheometry data with a Herschel–Bulkley model, during the unloading phase to be consistent with earlier thixotropic material experiments (Coussot, 1997; Roussel *et al.*, 2004; Chanson *et al.*, 2006):

$$\tau = \tau_c + \mu \times \left(\frac{\partial V}{\partial y}\right)^m \quad (1)$$

where τ is the shear stress, $\partial V/\partial y$ is the shear rate and the exponent m satisfies $0 < m \leq 1$ (Huang and Garcia, 1998; Wilson and Burgess, 1998). A comparison between experimental data and Equation (1) yielded results in terms of the yield stress, effective viscosity and exponent m listed in Table II. On average, the apparent viscosity was 4.5 Pa.s, the yield stress was about 5.9 Pa and $m \sim 0.228$ for the sediment sample collected on 19 October 2013 at low tide. The repeatability of the rheometry tests was checked by testing identically different samples; the results were very close as seen in Table II. Present findings of $\tau_c = 5$ to 6 Pa were comparable with previous investigations at the same site (Chanson *et al.*, 2011; Reungoat *et al.*, 2014a; Table II), although the data were quantitatively consistent with the qualitative observation of softer sediment samples.

The relationships between backscatter amplitude of ADV and OBS units and suspended sediment concentrations (SSCs) were tested systematically in two laboratories (University of Bordeaux and University of Leeds), for SSCs between 0 and 100 kg/m^3. The experimental results are summarised in Figure 4. The data showed similar qualitative trends for the OBS and ADV units: the data indicated a monotonic increase in suspended sediment concentration with increasing backscatter amplitude for SSC less than 2 to 10 kg/m^3. For larger SSCs (i.e. SSC > 10 kg/m^3), the experimental results showed a decreasing backscatter amplitude with increasing SSC, although

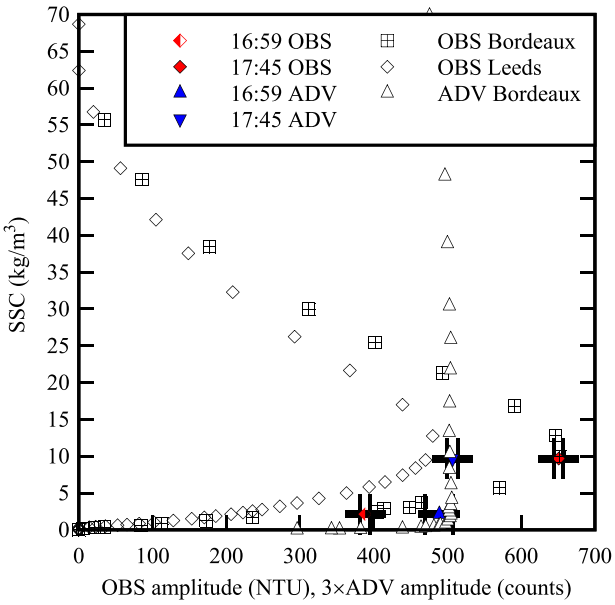

Figure 4. Relationship between suspended sediment concentration and backscatter amplitude for the sediment samples collected in the Arcins channel on 19 and 20 October 2013. Comparison between laboratory data (Bordeaux, Leeds) and sediment-laden water samples collected on 19 October 2013 (coloured symbols with error bars). This figure is available in colour online at wileyonlinelibrary.com/journal/espl

it was more significant with the OBS data. The general trends were consistent with a number of studies, including with cohesive sediment materials (Downing *et al.*, 1995; Ha *et al.*, 2009; Chanson *et al.*, 2011; Guerrero *et al.*, 2011; Brown and Chanson, 2012). Sediment-laden water samples were collected at Arcins in the Garonne River on 19 October 2013 before and after the tidal bore and analysed subsequently in both laboratories. The samples indicated a low suspended sediment concentration prior to the tidal bore, with SSC about 2 kg/m^3 at 16:59; a higher SSC, about 9.5 kg/m^3, was seen at 17:45, about 40 min after the bore passage. The sediment-laden water sample data analyses were compared with the calibration data of the ADV and OBS units in Figure 4 (error bars added for completeness). The results exhibited a reasonable agreement between the measured SSCs and ADV and OBS backscatter readings for both water samples, implying that the backscatter amplitude outputs may be used as a surrogate of SSC with the proper selection of some calibration curve. All the field observations indicated that the suspended sediment concentrations (SSCs) were very low prior to the tidal bore, while much larger sediment concentration levels were observed during and after the passage of the tidal bore. As a result, the SSC estimates were calculated using the following OBS calibration curve for SSC < 6 kg/m^3:

$$\begin{aligned} &SSC = 0.235 \times 1.0039^{NTU} \times NTU^{0.147} \\ &SSC < 6\ kg/m^3 (OBS) \end{aligned} \quad (2)$$

where the OBS backscatter amplitude (NTU) is in nephelometric turbidity units, and the suspended sediment concentration (SSC) is in kg/m^3. During and after the passage of the tidal bore, the SSCs were significantly larger and the OBS backscatter amplitude was attenuated by the heavily sediment-laden flow. The suspended sediment estimates were deduced from the OBS calibration data for SSC > 10 kg/m^3:

$$\begin{aligned} &SSC = 59.26 \times e^{-0.00226 \times NTU} \\ &SSC > 10\ kg/m^3 (OBS) \end{aligned} \quad (3)$$

Equations (2) and (3) were applied to the field data set before and after tidal bore passage, respectively. The results are presented and discussed below.

The velocity and SSC data were used to calculate the instantaneous suspended sediment flux per unit area $q_s = SSC \times V_x$ where q_s and V_x are positive in the downstream direction, SSC is in kg/m^3, and the sediment flux per unit area q_s is in kg/m^2/s. Herein the suspended sediment concentration (SSC) was estimated from the median OBS data and the longitudinal velocity was averaged over 5 s.

Results

Flow patterns and observations

The tidal bore formed at the downstream end of the Arcins channel and extended across the entire channel width. The bore shape evolved in response to the local bathymetry as the bore propagated upstream. It was undular at the sampling location (Figure 2(A) and (5)) and the bore front was well highlighted by two experienced surfers riding ahead of the first wave crest. The free-surface elevation rose very rapidly by 0.3 m in the first 10–15 s (Figure 6). For the next 60 s, the water elevation rose further by 1.1 m. The bore passage was immediately followed by a series of secondary waves lasting for a couple of minutes, with a wave period of about 1 s. During the field study, the water temperature varied from 18.7 °C to 17.9 °C and the water conductivity ranged from 25 mS/cm to 31 mS/cm depending upon the instrument, although each sensor data varied within only 2 mS/cm. The pH data ranged from 7.6 down to 7 with a monotonic decrease in pH during the afternoon. Importantly the present observations indicated an absence of a saline front, temperature front or pH front, associated with the tidal bore passage in the Arcins channel.

While the tidal bore advanced in the Arcins channel, another bore progressed into the main channel of the Garonne River (Figure 3). During the current field study, the bore of the main channel entered the Arcins channel at its upstream end, forming a marked bore propagating northwards (i.e. downstream) against the flood tide (Figure 5(C)). As the Arcins channel tidal bore approached the upstream end of the channel, it collided with the 'backward' bore of the main channel about 3 min. 53 s after it passed the sampling site (Figure 5(C)). Figure 3 presents a plan view sequence of the process, with the sketch No. 3 corresponding to a situation shortly prior to the bore collision seen in Figure 5(C). The tidal bore collision was experienced first hand by the two surfers seen in Figure 5(C): when the two bores collided, one surfer kneeled on his board while the second surfer remained standing but moved closer to the right bank (i.e. eastern bank). They described the bore collision as a very turbulent standing wave, associated with a rapid water level rise (Reungoat *et al.*, 2014b). While both surfers continued to surf the bore front southwards, their absolute speed dropped sharply as the standing wave formed and was almost stationary. Bestehorn and Tyvand (2009) provided a mathematical description for the formation of such a standing wave, after the collision of two undular bores. The bore collision generated a very dark black water mixing zone, evidence of massive sediment convection to the free-surface (Figure 5(C)). The collision was a unique experience for these two experienced tidal bore surfers.

After collision, the tidal bore of the Garonne River main channel continued to propagate downstream against the flood tide in the Arcins channel, with wave breaking seen next to the left and right banks (Figure 5(D)). In Figure 3 Right, the sketch No. 4 corresponds to the situation seen in Figure 5(D). The celerity of this 'backward' bore was between 1.5 and 2.5 m/s, compared with the celerity of the Arcins channel tidal bore of 4.3 m/s. The 'backward' bore reached the sampling station 9 min 32 s after the Arcins channel bore passed the ADV unit and continued until it reached the downstream end of the Arcins channel, where it vanished as the channel expanded. At the sampling station, the passage of the 'backward' bore was felt by the authors, with a sudden flow deceleration, associated with a northward surface flow motion next to the right bank and very strong turbulence next to the pontoon.

Velocity measurements

The instantaneous velocity components were measured prior to, during and after the tidal bore. The entire data set is reported in Figure 6, with the longitudinal velocity component V_x positive downstream. The time-variations of the water depth are included as well as the surface velocity data recorded using floating debris and stop watches on the channel centreline. Both the centreline surface velocity and ADV velocity data were very close prior to the bore passage: at the end of ebb tide, the current velocity was about +0.1 m/s, immediately prior to the bore passage. The tidal bore passage (t = 61 518 s) induced a marked effect on the longitudinal velocity (Figure 6). The current reversed its direction and the longitudinal velocity component was negative, between –0.8 and –1.2 m/s, at the ADV

Figure 5. Tidal bore of the Garonne River in the Arcins channel on 19 October 2013. (A) Approaching bore, looking downstream about 17:06 (white arrows points to longitudinal bed forms); (B) upstream propagation of undular bore at 17:07; (C) tidal bore collision at 17:10:15; (D) upstream propagation of 'backward' bore (white arrow) of the Garonne River in the Arcins channel at 17:15:13. This figure is available in colour online at wileyonlinelibrary.com/journal/espl

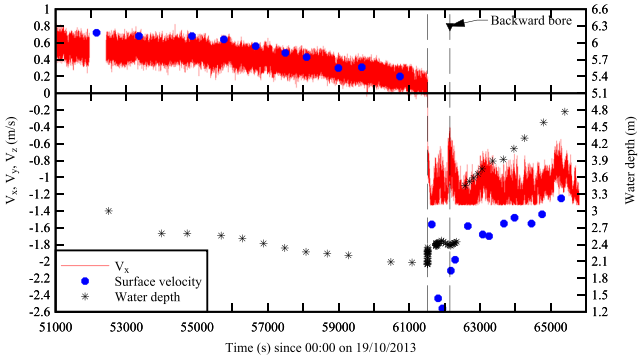

Figure 6. Time variations of instantaneous longitudinal velocity component and water depth in the Arcins channel on 19 October 2013. Post-processed ADV data (sampling rate: 200 Hz) and surface velocity on the channel centreline. Dashed lines mark the passage of the tidal bore and 'backward' bore. This figure is available in colour online at wileyonlinelibrary.com/journal/espl

sampling location. For comparison, the surface velocity on the channel centreline ranged between –1.2 and –2.6 m/s. The ADV sampling volume was located about 3 m from the right bank slope at low tide, and the slower ADV velocity data might reflect the effect of river bank boundary proximity. The passage of the bore was associated with large fluctuations of all three velocity components, including during the early ebb tide (Figure 6). About 570 s after the bore passage, the 'backward' bore of the main Garonne River channel reached the ADV unit. Its effect was felt with a drop in water elevation as well as a slower upstream flow motion, illustrated in Figure 6. (In Figure 6, the vertical dashed lines show the arrival of the tidal bore and 'backward' bore.) The flow deceleration experienced during the passage of the 'backward' bore may be predicted theoretically in the case of colliding bores, once the smaller 'backward' bore continues downstream. Large fluctuations of all velocity components were recorded during the 'backward' bore event ($62\ 100 < t < 62\ 300$ s, Figure 6). Altogether the propagation of the 'backward' bore induced some intense turbulent mixing, in addition to the strong surface mixing observed visually next to the right and left banks.

Turbulent Reynolds stress measurements

A turbulent Reynolds stress is proportional to the product of two velocity fluctuations, where the turbulent velocity fluctuation v is the deviation of the instantaneous velocity from an average $\overline{V}$. Herein $\overline{V}$ was the low-pass filtered velocity component, or

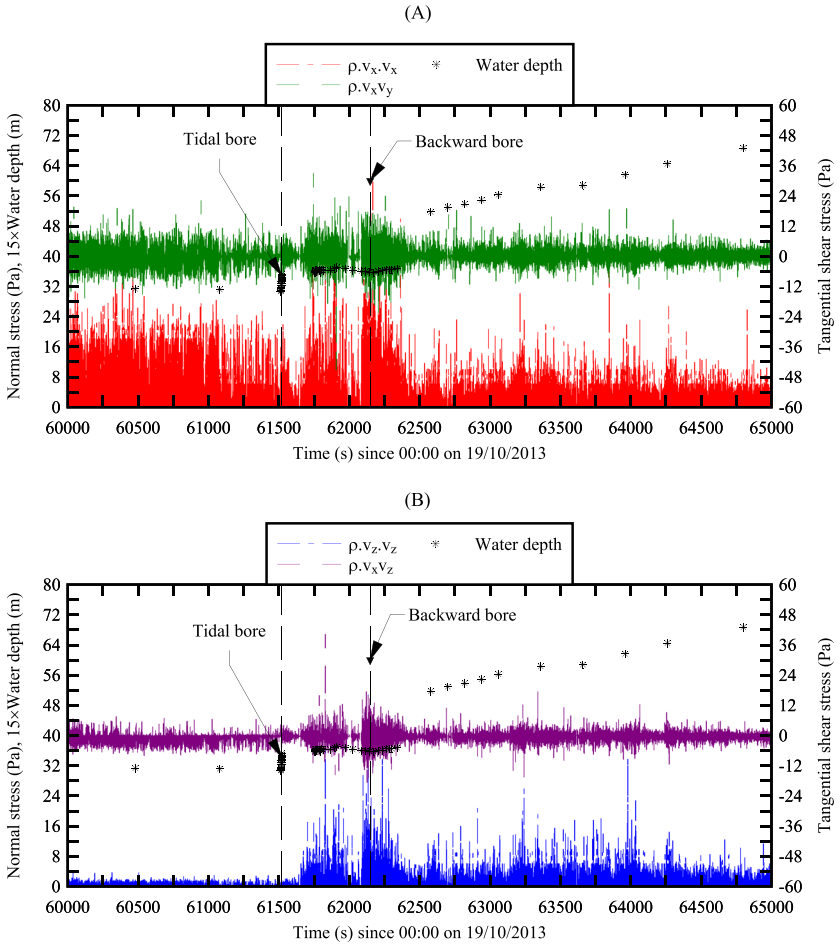

Figure 7. Time-variations of Reynolds stresses and water depth during the tidal bore passage on 19 October 2013. Post-processed ADV data, sampling rate: 200 Hz. Dashed lines mark the passage of the tidal bore and 'backward' bore. (A) $\rho \times v_x^2$ and $\rho \times v_x \times v_y$; (B) $\rho \times v_z^2$ and $\rho \times v_x \times v_z$. This figure is available in colour online at wileyonlinelibrary.com/journal/espl

variable interval time average VITA (Piquet, 1999; Chanson and Docherty, 2012). The cut-off frequency F_{cutoff} was derived based upon a sensitivity analysis conducted between an upper limit of the filtered signal (herein 100 Hz, the Nyquist frequency) and a lower limit corresponding to a period of about 0.96 s of the bore undulations. The results yielded an optimum threshold of $F_{cutoff} = 2$ Hz. The filtering was applied to all velocity components and the turbulent Reynolds stresses were calculated from the high-pass filtered signals. Typical results are presented in Figure 7.

The field observations showed large turbulent shear stresses, and large and rapid fluctuations in shear stresses during and after the tidal bore, for all Reynolds stress tensor components. The data highlighted also large magnitudes of shear stresses at about the time of passage of the 'backward' bore (Figure 7, t = 62 149 s). The turbulent shear stresses were significantly larger after the tidal bore passage: the mean normal stresses were four to sixteen times larger after the tidal bore passage than before, the standard deviations of all stress components were two to ten times larger after the tidal bore passage, and the maximum instantaneous Reynolds shear stresses were two to three times larger after the tidal bore. Herein maximum instantaneous shear stress amplitudes of up to 94 Pa were recorded, shortly (a few min) after the passage of the 'backward' bore. The data implied that the bore has the potential to scour the natural bed, with instantaneous stresses significantly larger than the material yield stress τ_c which is related to the minimum boundary shear stress required to erode and re-suspend cohesive sediments (Otsubo and Muraoko, 1988; Van Kessel and Blom, 1998). The tidal bore most likely scoured the channel bed and advected into suspension the bed material and carried the suspended sediments, behind the bore front during the early flood tide. This process applied to a significant length of the estuarine section of the Garonne River and would mobilise an enormous amount of sediments.

Suspended sediment processes

The time-variations of suspended sediment concentration (SSC) estimates were deduced from the OBS data and are presented in Figure 8(A). Note that the present data were median data calculated over 5 s. The water depth data are shown also in Figure 8(A) as well as the sediment concentrations of water samples tested in laboratory. The data showed some low SSC, 2.6 kg/m^3 on average, at the end of the ebb tide and the findings were close to the laboratory data (SSC = 2.12 kg/m^3). The passage of the tidal bore was associated with large fluctuations in SSC estimates. The 'backward' bore event induced even larger SSCs and SSC fluctuations, consistent with the large turbulent stress levels generated during the 'backward' bore passage which delayed the deposit of sediments (Figure 8(A)). The finding was consistent with both the visual observations and the turbulent Reynolds stress data set. During the later flood tide, the SSC estimates tended to 13–15 kg/m^3 on average.

The instantaneous suspended sediment flux per unit area q_s data are presented in Figure 8(B). The sediment flux data indicated a downstream positive mass flux during the end of ebb

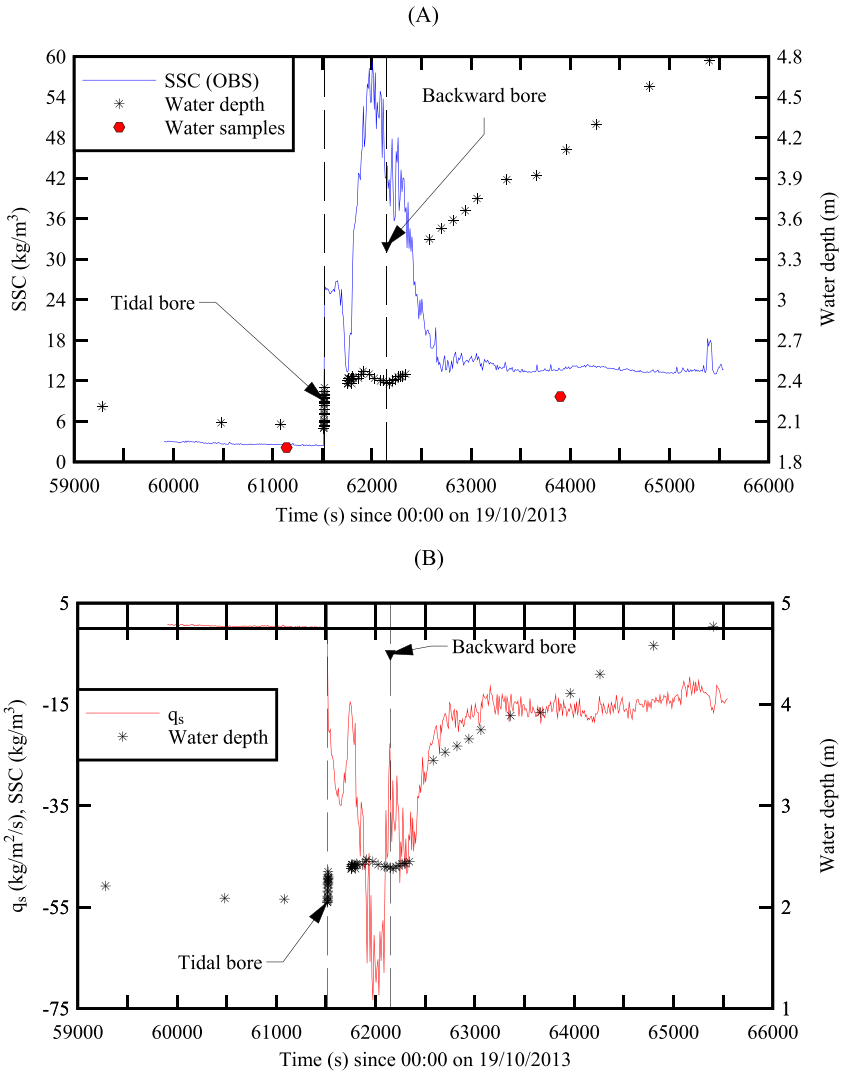

Figure 8. Time variations of suspended sediment concentration (SSC) estimate, mean suspended sediment flux per unit area and water depth on 19 October 2013. Median OBS data for 5 s and ADV data averaged over 5 s, all data returned every 10 s. Dashed lines mark the passage of the tidal bore and 'backward' bore. (A) Time variations of suspended sediment concentration (SSC) estimate; comparison with sediment-laden water sample data. (B) Time variations of the mean suspended sediment flux per unit area ($q_s = SSC \times V_x$). This figure is available in colour online at wileyonlinelibrary.com/journal/espl

tide. On average, the suspended sediment flux per unit area was 0.5 kg/m^2/s prior to the tidal bore. The tidal bore passage was characterised by a sudden flow reversal and the suspended sediment flux was negative during the flood tide. The sediment flux data q_s showed some large fluctuations. Shortly after the bore passage and during the 'backward' bore event, the sediment flux per unit reached very large mean negative values up to –73 kg/m^2/s (Figure 8(B)). About 45 min after the tidal bore, the sediment flux was –15 kg/m^2/s on average.

The sediment flux data were integrated with respect to time to yield the net sediment mass transfer per unit area during a given period. Prior the tidal bore ($60\,800 < t < 61\,511$ s), the net sediment mass transfer per unit area was +742 kg/m^2 for 12 min of data. Immediately following the tidal bore passage, the net sediment mass transfer equalled –39 970 kg/m^2 for 17 min ($61\,535 < t < 62\,574$ s). Towards the end of the study, the net sediment mass transfer equalled –32 000 kg/m^2 for 36 min ($63\,378 < t < 65\,530$ s). The data set highlighted the drastic impact of the 'backward' bore, not previously observed in earlier field studies. During the passage of the tidal bore and 'backward' bore event, the net sediment flux amplitude was about 38 times larger in magnitude than prior to the tidal bore, and 2.5 times larger than later during the flood tide.

Discussion

The downstream propagation of the 'backward' bore was a new feature which was not observed during previous field studies. It was believed to be linked with the recent siltation of the Arcins channel, which delayed the propagation of the tidal bore in the Arcins channel, since the bore celerity is proportional to the initial water depth:

$$U + V_1 \propto \sqrt{g \times \frac{A_1}{B_1}} \times \sqrt{1 + \varepsilon} \quad (4)$$

where ε is a term of second order (Tricker, 1965; Lighthill, 1978). The siltation of the Arcins channel might occur like the cutoff of secondary channels in meandering rivers (Doeglas, 1962; Parker *et al.*, 2011). The build-up of a low natural bar of hard materials was observed at the upstream end of the Arcins channel in mid-2013. It is conceivable that the major flood of the Garonne River in 2012 scoured the main channel, west of Arcins Island, reducing the ebb flow in the Arcins channel during low waters.

In October 2013, a feature of the river channel was a series of longitudinal rills along the right bank at low tide for most

Table III. Mean suspended sediment concentration SSC and mean suspended sediment flux per unit area q_s (kg s^{-1} m^{-2}) during the early flood tide immediately after the Garonne River bore at Arcins

Ref.	River system	Dates	SSC kg/m^3	q_s Kg s^{-1} m^{-2}	Comments
Present study	Garonne River	19 Oct. 2013	31.55	34.81	Bore passage and 'backward' bore
			13.9	15.21	After 'backward' bore
Reungoat *et al.* (2014a)	Garonne River	7 June 2012	31.7	24.7	
Chanson *et al.* (2011)	Garonne River	11 Sept. 2010	46.0	26.3	

of the length of the Arcins channel. Figure 5(A) illustrates such rills next to the sampling station (Figure 5(A), right with white arrow). The longitudinal forms looked like elongated, two-dimensional bed forms somehow similar to those reported by Carling *et al.* (2009) in the lower estuary of the River Severn, although with some key differences. The raised sections of River Severn were wider, with broader intermediary runnels and much longer runs. It is suggested that the bed form formation at Arcins was closely linked with some form of wash effect from the changing tide, the existence of the 'backward' bore flow and its induced turbulent mixing. Visual observations indicated that the elevation of the bed forms corresponded to the flooding induced by the 'backward' bore. Alternatively the longitudinal bed forms at Arcins could be possibly older drag marks induced by some large debris and preserved across several tides. At this stage, no definite conclusion can be drawn.

The present field data highlighted a significant suspended sediment load during the tidal bore, including during the 'backward' bore event. Table III regroups the results in terms of the mean suspended sediment concentration and average suspended sediment flux per unit area during the early flood tide. Two data sets are shown for the distinctively different periods: (a) during the tidal bore event and 'backward' bore; and (b) after the 'backward' bore. The present data were compared with the earlier suspended sediment load data in the Garonne River tidal bores in 2010 and 2012 (Chanson *et al.*, 2011; Reungoat *et al.*, 2014a). Any comparison between the present findings and earlier data in the Arcins channel must be considered with care, because of the difference in instrumentation and type of data (instantaneous vs average) (Table I). Altogether the present data showed large suspended sediment fluxes per unit area and SSCs observed during the Garonne River tidal bore and early flood tide. To date a few studies have highlighted the intense sediment mixing and upstream advection of suspended matters during the passage of a tidal bore (Chen *et al.*, 1990; Greb and Archer, 2007; Chanson *et al.*, 2011; Furgerot *et al.*, 2013; Reungoat *et al.*, 2014a). The present data set supported the same trend, and they showed further the drastic impact of tidal collision in terms of sediment processes.

The sediment deposit samples were predominantly silty material that exhibited a non-Newtonian behaviour under rheological testing (see above). The rheological properties of the sediment deposits were directly relevant to the inception of sediment materials and properties of the dilute suspension. The apparent yield stress of the mud provided some quantitative information on the critical shear stress for sediment erosion. Previous studies indicated that the critical shear stress for mud erosion and sediment re-suspension is close to and slightly lower than the yield stress (Otsubo and Muraoko, 1988; Van Kessel and Blom, 1998; Hobson, 2008; Sanchez and Levacher, 2008; Jacobs *et al.*, 2011). Once the fluid shear stress exceeds the local strength of the bed, surface erosion occurs initially, in the form of stripping and aggregate fragmentation (Pouv *et al.*, 2014). This is followed after some time by mass erosion, occurring rapidly (Amos *et al.*, 1992; Winterwerp and Van Kestere, 2004). In the laboratory, Pouv *et al.* (2014) observed bulk erosion about 7 to 40 min after the experiment start depending upon the test conditions. The same erosion processes were likely observed in the Arcins channel. It is believed that the passage of the tidal bore induced a drastic increase in fluid shear stress that induced immediately some surface erosion of the bed material, followed by delayed mass erosion. The latter would be consistent with the present observations of sediment upwelling and sediment flocs bursting at the free-surface for the next two hours, similar to observations by Chanson *et al.* (2011), as well as with the observations of fold-shaped and 'tobacco pouch'-shaped scour forms, cusps and depressions observed in France and Canada (Tessier and Terwindt, 1994; Faas, 1995).

Once the sediment bed material was eroded and entrained by the bore, the present rheological data implied that, at high suspended sediment concentrations, the flood tide waters might exhibit some non-Newtonian characteristics, and their behaviour cannot be predicted accurately without a detailed rheological characterisation of the sediment materials (Wang *et al.*, 1994; Antoine *et al.*, 1995; Coussot 1997, 2005; Brown and Chanson, 2012). Using dilute suspensions of bentonite, Chanson *et al.* (2006) showed a non-Newtonian thixotropic flow behaviour using both dam break wave experiment and rheometry data, while Coussot and Ovarlez (2010) demonstrated the non-Newtonian thixotropic behaviour of dilute suspensions of bentonite using direct magnetic resonance imaging (MRI). These results suggested a non-Newtonian behaviour of dilute suspensions for mass concentrations as low as 1%. During the present field investigation, SSC estimates between 10 kg/m^3 and 60 kg/m^3 were observed during the tidal bore and early flood tide (Figure 8(A)), corresponding to mass concentrations between 1 and 6%. The present SSC estimates, together with the sediment rheological data, implied that the early flood tide flow with high suspended sediment concentrations might exhibit some form of non-Newtonian flow behaviour. This has never been taken into account in conceptual and hydrodynamic models.

Conclusion

A detailed field study was conducted in the Garonne River at Arcins (France) to characterise the turbulent and sedimentary processes of the tidal bore. Key features of the investigation included the fine temporal resolution with a 200 Hz velocity sampling rate, the complementary nature of the instruments (ADV, OBS, CTD) and a comprehensive characterisation of the sediment properties including granulometry and rheology. The sediment samples were predominantly silty material with a median particle size about 15 μm and they exhibited a non-Newtonian thixotropic behaviour under rheological testing.

The tidal bore was undular and the undular front was followed by well-defined whelps with wave period about 1 s. A most unusual feature was the collision between the Arcins channel tidal bore and the bore of the Garonne River main

channel. The bore collision occurred close to the upstream end of the Arcins channel about 800 m from the sampling site. It was well-documented by two surfers and a number of photographs. The collision of the bores generated a transient standing wave with a dark blackwater mixing zone. The Garonne River main channel bore propagated 'backward' along the Arcins channel with some breaking next to the river bank. Its effects were felt at the sampling site with a temporary lowering of the water surface and flow deceleration.

The instantaneous velocity data indicated large Reynolds shear stresses observed during and after the tidal bore, including during the 'backward' bore propagation. Large SSC estimates were observed in the tidal bore and early flood tide. Based upon the rheological characteristics of bed material, it is proposed that the bore passage induced immediately some surface erosion followed by delayed bulk erosion. During the tidal bore passage, the 'backward' bore event, and the early flood tide, the suspended sediment flux data showed some substantial sediment suspension amplitudes consistent with the murky appearance of flood tide waters.

The collision of tidal bores in the Arcins channel was a most unusual occurrence. It is proposed that this phenomenon was caused by the relatively recent siltation of the Arcins channel, delaying the propagation of the tidal bore in the silted channel and allowing the main channel bore to enter and develop at the upstream end of the Arcins channel. All the quantitative data, sampled at 800 m north of the collision site, indicated a massive impact of the bore collision on the entire Arcins channel system.

Acknowledgements—The authors thank Dr Frédérique Larrarte (IFSTTAR Nantes) and Professor Michael Bestehorn (Brandenburg University of Technology) for their initial comments. They acknowledge the helpful inputs of Professor Dan Parsons (University of Hull), Professor Pierre Lubin (University of Bordeaux), Dr Eric Jones (Proudman Oceanographic Laboratory) and the journal reviewers. The authors acknowledge the assistance of Patrice Benghiati and the permission to access and use the pontoon in the Bras d'Arcins. They thank all the people who participated to the field works, and without whom the study could not have been conducted, and the SEFDL at the University of Leeds for the loan of equipment. They also thank Frédéric Daney (Bordeaux, France), and Daniel Leblanc (Moncton, Canada) for a number of useful discussions and information. The authors acknowledge the financial assistance of the Agence Nationale de la Recherche (Projet MASCARET 10-BLAN-0911-01).

References

Amos CL, Daborn GR, Christian HA, Atkinson A, Robertson A. 1992. *In situ* erosion measurements on fine grained sediments from the Bay of Fundy. *Marine Geology* **108**: 175–196. (DOI: 10.1016/0025-3227(92)90171-D).

Antoine P, Giraud A, Meunier M, Van Asch T. 1995. Geological and geotechnical properties of the 'Terres Noires' in southeastern France: weathering, erosion, solid transport and instability. *Engineering Geology* **40**: 223–234.

Bartsch-Winkler S, Emanuel RP, Winkler GR. 1985. Reconnaissance hydrology and suspended sediment analysis, Turnagain Arm estuary, upper Cook Inlet. In The United States Geological Survey in Alaska; accomplishments during 1984, Bartsch-Winkler S (ed). US Geological Survey Circular 967, 49–51.

Bestehorn M, Tyvand PA. 2009. Merging and Colliding Bores. *Physics of Fluids* **21**: 042107 (DOI: 10.1063/1.3115909).

Brown R, Chanson H. 2012. Suspended sediment properties and suspended sediment flux estimates in an urban environment during a major flood event. *Water Resources Research* AGU, Vol. **48**, Paper W11523 (DOI: 10.1029/2012WR012381).

Carling PA, Williams JJ, Croudace IW, Amos CL. 2009. Formation of mud ridge and runnels in the intertidal zone of the Severn estuary, UK. *Continental Shelf Research* **29**: 1913–1926 (DOI: 10.1016/j.csr.2008.12.009).

CBC News. 2013. 5 super bore surfers hit by surprise wave in Moncton. http://www.cbc.ca/news/canada/new-brunswick/5-super-bore-surfers-hit-by-surprise-wave-in-moncton-1.2418096 (Webpage accessed on 2 Dec. 2013).

Chanson H 2011a. *Tidal Bores, Aegir, Eagre, Mascaret, Pororoca: Theory and Observations*. World Scientific: Singapore (ISBN 9789814335416).

Chanson H 2011b. Turbulent shear stresses in hydraulic jumps and decelerating surges: an experimental study. *Earth Surface Processes and Landforms* **36**(2): 180–189 and 2 videos (DOI: 10.1002/esp.2031).

Chanson H, Docherty NJ. 2012. Turbulent velocity measurements in open channel bores. *European Journal of Mechanics B/Fluids* **32**: 52–58 (DOI 10.1016/j.euromechflu.2011.10.001).

Chanson H, Jarny S, Coussot P. 2006. Dam break wave of thixotropic fluid. *Journal of Hydraulic Engineering ASCE* **132**: 280–293 (DOI: 10.1061/(ASCE)0733-9429(2006)132:3(280)).

Chanson H, Takeuchi M, Trevethan M. 2008. Using turbidity and acoustic backscatter intensity as surrogate measures of suspended sediment concentration in a small sub-tropical estuary. *Journal of Environmental Management* **88**: 1406–1416 (DOI: 10.1016/j.jenvman.2007.07.009).

Chanson H, Reungoat D, Simon B, Lubin P. 2011. High-frequency turbulence and suspended sediment concentration measurements in the Garonne river tidal bore. *Estuarine, Coastal and Shelf Science* **95**: 298–306 (DOI 10.1016/j.ecss.2011.09.012).

Chen J, L Ci, Zhang C, Walker HJ. 1990. Geomorphological development and sedimentation in Qiantang estuary and Hangzhou bay. *Journal of Coastal Research* **6**: 559–572.

Chen S 2003. Tidal bore in the north branch of the Changjiang estuary. Proceedings of the International Conference on Estuaries and Coasts ICEC - 2003, Hangzhou, China, Nov. 8–11, International Research and Training Center on Erosion and Sedimentation. Vol. **1**, pp. 233–239.

Coussot P. 1997. *Mudflow Rheology and Dynamics*. IAHR Monograph, Balkema: The Netherlands.

Coussot P. 2005. *Rheometry of Pastes, Suspensions, and Granular Materials. Applications in Industry and Environment*. John Wiley: New York.

Coussot P, Overlez G. 2010. Physical origin of shear-banding in jammed systems. *The European Physical Journal E* **33**(3): 183–188. (DOI: 10.1140/epje/i2010-10660-9).

Doeglas DJ. 1962. The structure of sedimentary deposits of braided rivers. *Sedimentology* **1**: 167–193.

Downing A, Thorne PD, Vincent CE. 1995. Backscattering from a suspension in the near field of a piston transducer. *Journal of Acoustical Society of America* **97**: 1614–1620.

Faas RW. 1995. Rheological constraints on fine sediment distribution and behavior: the Cornwallis estuary, Novia Scotia. Proceedings of the Canadian Coastal Conference, Dartmouth, Nova Scotia, pp. 301–314.

Fan D, Tu J, Shang S, Cai G. 2014. Characteristics of tidal-bore deposits and facies associations in the Qiantang Estuary, China. *Marine Geology* **348**: 1–14 (DOI: 10.1016/j.margeo.2013.11.012).

Furgerot L, Mouaze D, Tessier B, Perez L, Haquin S. 2013. Suspended sediment concentration in relation to the passage of a tidal bore (Sée River Estuary, Mont Saint Michel, NW France). Proceedings of Coastal Dynamics 2013, Arcachon, France, 24–28 June, pp. 671–682.

Graf WH. 1971. *Hydraulics of Sediment Transport*. McGraw-Hill: New York.

Greb SF, Archer AW. 2007. Soft-sediment deformation produced by tides in a meizoseismic area, Turnagain Arm, Alaska. *Geology* **35**: 435–438.

Guerrero M, Szupiany RN, Amsler M. 2011. Comparison of acoustic backscattering techniques for suspended sediments investigation. *Flow Measurement and Instrumentation* **22**: 392–401.

Ha HK, Hsu WY, Maa JPY, Shao YY, Holland CW. 2009. Using ADV backscatter strength for measuring suspended cohesive sediment concentration. *Continental Shelf Research* **29**: 1310–1316.

Hobson PM. 2008. Rheologic and flume erosion characteristics of georgia sediments from bridge foundations. MSc thesis, School of Civil and Environmental Engineering, Georgia Institute of Technology.

Huang X, Garcia M. 1998. A Herschel-Bulkley model for mud flow down a slope. *Journal of Fluid Mechanics* **374**: 305–333.

Jacobs W, Le Hir P, Van Kesteren W, Cann P. 2011. Erosion threshold of sand–mud mixtures. *Continental Shelf Research* **31**: S14–S25 (DOI: 10.1016/j.csr.2010.05.012).

Julien PY. 1995. *Erosion and Sedimentation*. Cambridge University Press: Cambridge.

Khezri N, Chanson H. 2012a. Undular and breaking tidal bores on fixed and movable gravel beds. *Journal of Hydraulic Research IAHR* **50**: 353–363 (DOI: 10.1080/00221686.2012.686200).

Khezri N, Chanson H. 2012b. Inception of bed load motion beneath a bore. *Geomorphology* **153–154**: 39–47 (DOI: 10.1016/j.geomorph.2012.02.006).

Khezri N, Chanson H. 2015. Turbulent velocity, sediment motion and particle trajectories under breaking tidal bores: simultaneous physical measurements. *Environmental Fluid Mechanics* **15**: (DOI: 10.1007/s10652-014-9358-z) (Online First).

Kjerfve B, Ferreira HO. 1993. Tidal bores: first ever measurements. *Ciência e Cultura (Journal of the Brazilian Association for the Advancement of Science)* **45**(2): 135–138.

Lewis AW. 1972. Field studies of a tidal bore in the River Dee. MSc thesis, Marine Science Laboratories, University College of North Wales, Bangor, UK.

Ligget, JA. 1994. *Fluid Mechanics*. McGraw-Hill: New York.

Lighthill J. 1978. *Waves in Fluids*. Cambridge University Press: Cambridge.

Macdonald RG, Alexander J, Bacon JC, Cooker MJ. 2009. Flow patterns, sedimentation and deposit architecture under a hydraulic jump on a non-eroding bed: defining hydraulic-jump unit bars. *Sedimentology* **60**: 1291–1312.

Malandain JJ. 1988. La Seine au Temps du Mascaret. (The Seine River at the Time of the Mascaret). *Le Chasse-Marée* **34**: 30–45 (in French).

Moore RN. 1888. *Report on the Bore of the Tsien-Tang Kiang*. Hydrographic Office: London.

Mouaze D, Chanson H, Simon B. 2010. Field measurements in the tidal bore of the Sélune River in the Bay of Mont Saint Michel (September 2010). Hydraulic Model Report No. CH81/10, School of Civil Engineering, The University of Queensland, Brisbane, Australia (ISBN 9781742720210).

Navarre P. 1995. Aspects Physiques du Caractère Ondulatoire du Macaret en Dordogne. (Physical features of the undulations of the Dordogne River tidal bore.) DEA thesis, University of Bordeaux, France (in French).

Otsubo K, Muraoko K. 1988. Critical shear stress of cohesive bottom sediments. *Journal of Hydraulic Engineering ASCE* **114**: 1241–1256.

Parker G, Shimizu Y, Wilkerson GV, Eke EC, Abad JD, Lauer JW, Paola C, Dietrich WE, Voller VR. 2011. A new framework for modeling the migration of meandering rivers. *Earth Surface Processes and Landforms* **36**: 70–86.

Peregrine DH. 1966. Calculations of the Development of an Undular Bore. *Journal of Fluid Mechanics* **25**: 321–330.

Piquet J. 1999. *Turbulent Flows. Models and Physics*. Springer: Berlin.

Pouv KS, Besq A, Gullou SS, Toorman EA. 2014. On cohesive sediment erosion: a first experimental study of the local processes using transparent model materials. *Advances in Water Resources* **72**: 71–83.

Ramsden JD. 1996. Forces on a vertical wall due to long waves, bores and dry-bed surges. *Journal of Waterway Port Coastal and Ocean Engineering ASCE* **122**: 134–141.

Reungoat D, Chanson H, Caplain B. 2014a. Sediment processes and flow reversal in the undular tidal bore of the Garonne river (France). *Environmental Fluid Mechanics* **14**: 591–616 (DOI: 10.1007/s10652-013-9319-y).

Reungoat D, Chanson H, Keevil C. 2014b. Turbulence, sedimentary processes and tidal bore collision in the Arcins channel, Garonne river (October 2013). Hydraulic Model Report No. CH94/14, School of Civil Engineering, The University of Queensland, Brisbane, Australia (ISBN 9781742721033).

Roussel N, Le Roy R, Coussot P. 2004. Thixotropy modelling at local and macroscopic scales. *Journal of Non-Newtonian Fluid Mecheanics* **117**: 85–95.

Rowbotham F 1983. *The Severn Bore*, 3rd edn. David and Charles: Newton Abbot, UK.

Sanchez M, Levacher D. 2008. Erosion d'une vase de l'estuaire de la Loire sous l'action du courant. (Erosion of a mud from the Loire estuary by a flow). *Bulletin of English Geology Environment* **67**: 597–605 (DOI: 10.1007/s10064-008-0159-9).

Simpson JH, Fisher NR, Wiles P. 2004. Reynolds stress and TKE production in an estuary with a tidal bore. *Estuarine, Coastal and Shelf Science* **60**: 619–627.

Stoker JJ. 1957. *Water Waves. The Mathematical Theory with Applications*. Interscience Publishers: New York.

Tessier B, Terwindt JHJ. 1994. An example of soft-sediment deformations in an intertidal environment - the effect of a tidal bore. *Comptes-Rendus de l'Académie des Sciences* Série II, Vol. **319**(2), Part 2: 217–233 (in French).

Tricker RAR. 1965. *Bores, Breakers, Waves and Wakes*. American Elsevier Publishing Co: New York.

Van Kessel T, Blom C. 1998. Rheology of cohesive sediments: comparison between a natural and an artificial mud. *Journal of Hydraulic Research IAHR* **36**: 591–612.

Wang ZY, Larsen P, Xiang W. 1994. Rheological properties of sediment suspensions and their implications. *Journal of Hydraulic Research, IAHR* **32**: 495–516.

Wilson SDR, Burgess SL. 1998. The steady, spreading flow of a rivulet of mud. *Journal of Non-Newtonian Fluid Mechanics* **79**: 77–85.

Winterwerp JC, Van Kesteren WGM. 2004. *Introduction to the Physics of Cohesive Sediment in the Marine Environment*. Elsevier, Developments in Sedimentology, Van Loon T (ed). Elsevier: Amsterdam.

Wolanski E, Moore K, Spagnol S, D'adamo N, Pattieratchi C. 2001. Rapid, human-induced siltation of the macro-tidal Ord river estuary, western Australia. *Estuarine, Coastal and Shelf Science* **53**: 717–732.

Wolanski E, Williams D, Spagnol S, Chanson H. 2004. Undular tidal bore dynamics in the Daly estuary, Northern Australia. *Estuarine, Coastal and Shelf Science* **60**: 629–636.